RSC Advances

PAPER

View Article Online
View Journal | View Issue

Cite this: *RSC Adv.*, 2021, **11**, 15036

Application of a blast furnace slag carrier catalyst in flue gas denitration and sulfur resistance

Zhang Lei, *[ad] Lu Xi,[a] Qi Lingbo,[a] Shu Hao,[b] Jia Yang,[b] Lei Zhang,[c] Yan Yao[a] and Bai Fang[e]

Received 28th January 2021
Accepted 3rd March 2021

DOI: 10.1039/d1ra00752a

rsc.li/rsc-advances

It is an urgent need to develop a new catalyst with high efficiency and low cost. In the present study, we successfully prepared bimetallic-supported denitration catalysts using the blast furnace slag as the main material and calcium bentonite as the binder. The as-prepared catalyst was characterized *via* X-ray diffraction analysis (XRD), Fourier transform infrared spectroscopy (FTIR), and scanning electron microscopy (SEM). Besides, the mechanism of denitration was further determined with the help of the denitration and sulfur resistance of the catalyst. The results indicated that when the Mn load was 5%, and the second metal reactive component was loaded at 3%, Mn–Cu/GGBS (catalyst prepared by loading Mn and Cu on the blast furnace slag) had the best effects on low temperature denitration. Moreover, the conversion rate of NO was up to 97%, and it possessed the capability of specific sulfur resistance; when the third metal reactive component, Ce, was introduced with 1% load, the sulfur resistance of the Mn–Cu–Ce/GGBS (catalyst prepared by loading Mn, Cu, and Ce on the blast furnace slag) catalyst was further improved compared with that of the Mn–Cu/GGBS catalyst.

1. Introduction

Nitrogen oxides (NO_x), the main air pollutants, mainly come from the combustion of coal and fossil fuels.[1–3] We know that a large proportion of these emissions are from coal-fired power plants. In order to reduce pollution, one of the technologies adopted by most coal-fired power plants is selective catalytic reduction denitration, and the core of the SCR technology is the catalyst.[2–5] Although some progress has been made in the study of SCR catalysts, the denitration catalyst is expensive and its sulfur resistance is insufficient.[6–9] Consequently, the preparation of high performance denitration and sulfur-resistant catalysts characterized by high efficiency, simplicity, and energy conservation has become a hot topic in this field.[10–12]

There are numerous types of catalysts in the world. For example, the SCR catalyst commonly used in industry is the vanadium-titanium catalyst, and this kind of catalyst tends to be poisonous and deactivated.[13,14] Furthermore, the temperature window is wide, and V_2O_5 (one of the SCR catalysts) is highly poisonous.[15–18] Therefore, it is necessary to develop a new catalyst with less pollution, low cost, and high efficiency.[19] Zhang *et al.*[20] successfully synthesized a $V_2O_5/Sn_xTi_{1-x}O_2$ catalyst by means of impregnation. Compared with the conventional V_2O_5/TiO_2 (anatase) catalyst, $V_2O_5/Sn_{0.2}Ti_{0.8}O_2$ has better low temperature SCR activity and better resistance to H_2O and SO_2. Taking Ce–TiO_2 as the carrier, an active component, V_2O_5–WO_3, was impregnated in the carrier by precipitation, and A. Kubilay[21] finally prepared a V_2O_5–WO_3/Ce–TiO_2 catalyst and tested its denitration. It turned out that when there was a 250–475 °C temperature window and the conversion rate of NO_x could reach more than 80%. The optimal reaction temperature was at 325 °C, and the denitration efficiency could reach up to 99% at that moment. According to the chemical deposition, Liu *et al.*[22] prepared a CeO_2–MnO_x catalyst with a special core–shell structure, which was also characterized and tested for its denitration and activity. The result showed that when CeO_2/MnO_x ratio was 0.6 and the reaction temperature remained 110–220 °C, the NO_x conversion rate was relatively high.[23–27] Because of its special structure, the catalyst showed better sulfur resistance. However, most of these catalysts are powdery with poor mechanical properties, short service life, and high preparation cost.[27–29]

Blast furnace slag (GGBS) is a main industrial by-product during the process of blast furnace smelting of pig iron.[30–32] There are CaO,[33] MgO,[34] SiO_2,[35] Al_2O_3,[36] Fe_2O_3,[37] and other oxide

[a]*Xi'an University of Science and Technology, Xi'an, 710054, China. E-mail: 136750178@qq.com; 1029571241@qq.com; 759809714@qq.com; 634122318@qq.com; Tel: +8618502993567*

[b]*Xi'an University of Technology, Xi'an, 710048, China. E-mail: 490258879@qq.com; 519322049@qq.com*

[c]*China National Heavy Machinery Research Institute Co, Ltd, Xi'an, 710032, China. E-mail: leizh666@sohu.com*

[d]*Key Laboratory of Coal Resources Exploration and Comprehensive Utilization, Ministry of Natural Resources, Xi'an, 710021, China*

[e]*CAS Key Laboratory of Green Process and Engineering, Institute of Process Engineering, Chinese Academy of Sciences, Beijing, 100190, China. E-mail: fbai@ipe.ac.cn*

compositions accounted for more than 80%, so it is a type of mineral resource with high recycling value.[38–42] With the rapid development of the steel industry, the mounting of slag emissions is visible. Therefore, a series of environmental problems exist in our life. For example, if slag is not emptied out in time, there will be a wide-occupation area and a large amount of accumulation.[43] Rain also scours slag so that groundwater is polluted. Besides, the dust produced by the blow of slag endangers people's health. In order to make the slag resource effective, scholars in this field both at home and abroad take great advantage of the slag to make construction materials, cementitious materials, and others.[44] In addition, blast furnace slag is also a cheap catalyst, widely used in the environmental sewage treatment, industrial catalyst preparation, soil remediation, and other fields.[45]

In this study, bentonite was used as a binder and transition metals as reactive components. The authors chose the blast furnace slag as the main raw material for the first time and prepared a low-cost, high-strength bimetallic blast furnace slag catalyst through equal volume impregnation. On the basis of equal volume impregnation, the blast furnace slag and bentonite were used as materials. The authors again successfully prepared a series of supported denitration catalysts. XRD, FT-IR, SEM, and other methods were used to characterize the catalyst. The denitration and sulfur resistance were also investigated. It turned out that the supported blast furnace slag-based catalyst has a good removal effect on NO_x in flue gas and has good sulfur resistance. In summary, this research provides a clear research direction to find a low-cost and not easily powdered denitration sulfur-resistant catalyst. Simultaneously, it has achieved the goal of treating waste with waste and turning waste into treasure. Finally, it lays a theoretical foundation for the study of low-cost denitration sulfur-resistant catalysts in the future.

2. Materials and methods

2.1. The preparation of the catalyst

The blast furnace slag powder used in the experiment was obtained from a steel plant in Hanzhong, Shaanxi Province. The bentonite was produced by Tianyuan Non-metallic Products Co., Ltd and used without further purification. We mainly studied the formation of a blast furnace slag catalyst and the loading of different metals. The process was as follows: quantified blast furnace slag powder and calcium bentonite were mixed according to a mass ratio of 4 : 1 in a beaker, 30 wt% of distilled water was added, stirred, and made a mass with specific humidity. The sample was loaded into the extruder. The extruded sample was kept in a 105 °C oven and dried for 1 h. After cooling, the sample was cut into a cylindrical carrier (equal height 5 mm) to reserve. Mn was mixed with nitrates from different metals proportionately. Mn was loaded at 5%, and the second metal (Cr, Co, Ni, Cu, Zn, Ag, Cd, and Fe) was loaded at 3%, *via* the same volume impregnation method. The blast furnace slag carrier was impregnated in a configured solution for 24 h and then taken out. The temperature of the drying box was adjusted to be 105 °C, and the loaded blast furnace slag base carrier was placed in a constant temperature drying box for drying. There was 15 minutes before it could be taken out. A series of catalysts could be prepared by 450 °C roasting for 2 h in a muffle furnace. These were Mn–Fe/GGBS, Mn–Co/GGBS, Mn–Ni/GGBS, Mn–Cr/GGBS, Mn–Cu/GGBS, Mn–Zn/GGBS, Mn–Ag/GGBS, and Mn–Cd/GGBS.

2.2. The evaluation of catalyst activity

2.2.1 Experimental equipment. The evaluation of catalyst activity was carried out in the simulated flue gas unit, as shown in Fig. 1. By infusing the simulated gas, the change of its NO data was observed.

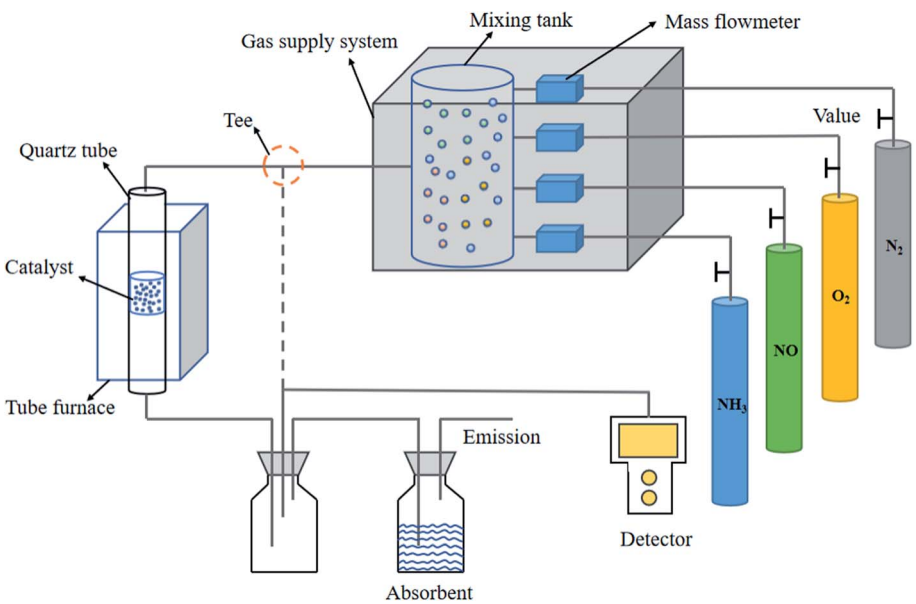

Fig. 1 Catalyst evaluation unit.

2.2.2 The steps and methods of evaluation unit operation. A constant temperature of 150 °C was set in a tubular furnace, and the temperature programming was adopted in the process of temperature rising. Accordingly, there was no over-heating in a tubular furnace and further made sure that the reaction was within the normal temperature. The gas supply system was turned on, and the total ventilation volume was 500 mL min^{-1}. O_2 flow was set at 6% (30 mL min^{-1}), NH_3 at 544 ppm (8 mL min^{-1}), NO at 544 ppm (8 mL min^{-1}), and the remaining filling gas N_2 was at 454 mL min^{-1}. As the system was introduced into SO_2, O_2 was set at 6% (30 mL min^{-1}), NH_3 at 544 ppm (8 mL min^{-1}), NO at 544 ppm (8 mL min^{-1}), SO_2 at 160 ppm (2 mL min^{-1}), and the remaining filling gas N_2 was at 452 mL min^{-1}. A Testo probe was inserted into the bypass, and the data of NO could be observed, and the bypass was turned off when the data was stable. About 10 g of the as-prepared catalyst was put into the tube furnace in advance. Before the system became stable, the three links at the front of the tube furnace were closed. Then, the simulated gas was let into the main gas and tube furnace from the bypass, and the data of NO from the back of the tube furnace was recorded, collated, and collected. The recorded NO data was used in calculating the denitration efficiency of each catalyst. The formula was as follows:

$$x = \frac{C_{NO_{in}} - C_{NO_{out}}}{C_{NO_{in}}} \times 100\% \quad (1)$$

3. Results and discussions

3.1 Synthesis and characterization of catalytic materials

3.1.1 XRD analysis. As shown in Fig. 2, the main crystal structure of the Mn–Cu/GGBS catalyst had changed negligibly after denitration and sulfur resistance. It mainly took manganese oxides and copper oxides as crystal forms. Mn element existed in the form of MnO_2 and Mn_5O_8 oxides. However, the other valence manganese oxides were not crystalline, indicating that MnO, Mn_3O_4, and Mn_2O_3 are dispersed on the catalyst surface in an amorphous manner. Cu element existed as oxides of CuO. It means that Cu_2O existed in the amorphous form or as uniform dispersion. Mn and Cu elements also presented a crystal form $Cu_{0.451}Mn_{0.549}O_2$ (PDF#41-0184). With the help of the denitration effects of the bimetallic supported catalyst (Fig. 2), we know that the effect was improved significantly. Therefore, it further illustrated the synergistic effects between metallic manganese and the second reactive component. The main chemical components of the GGBS catalyst and bentonite are CaO, Al_2O_3, and SiO_2.

For GGBS, adding bentonite can increase the strength of the GGBS catalyst, and the SiO_2 diffraction peak at 27.348° significantly enhanced. For the Mn–Cu/GGBS (fresh) catalyst, the diffraction peaks at 18.111° and 19.531° are MnO_2 (PDF#44-0141) Mn_5O_8 (PDF#39-1218), and the diffraction peak at 35.262° is CuO (PDF#44-0706). The diffraction peak of the deactivated Mn–Cu/GGBS (deactivated) catalyst reduced, and the diffraction peak of MnO_2 at 18.111° is not obvious. The intensity of the diffraction peak of $Cu_{0.451}Mn_{0.549}O_2$ (PDF#41-0184) at 27.472° reduced. Before and after denitration and after sulfur resistance, the characteristic peak of the catalyst appeared at 65.573° (PDF#41-0184).

3.1.2 FT-IR analysis. The infrared spectra of the modified Mn/GGBS catalyst are shown in Fig. 3: Mn–Cu/GGBS (fresh), Mn–Cu/GGBS (inactivated), and Mn–Cu/GGBS (desulfurization). Water added to the catalyst during the formation process caused the hydration reaction in the slag, and calcium silicate reacted with water to form hydrate calcium silicate and calcium hydroxide. At 3649 cm^{-1}, the three catalysts showed the –OH stretching vibration peak of $Ca(OH)_2$ produced by hydration. The peak at 1427 cm^{-1} is the result of the Si–O bond stretching vibration of SiO_2 (amorphous phase) in the slag. The peak value weakened after the catalyst was prepared. For the blast furnace slag, there was a big concave peak, which was produced by the stretching vibration of Si–O at 1000 cm^{-1}. After the modification of the metal salt, this peak shifted towards the direction of

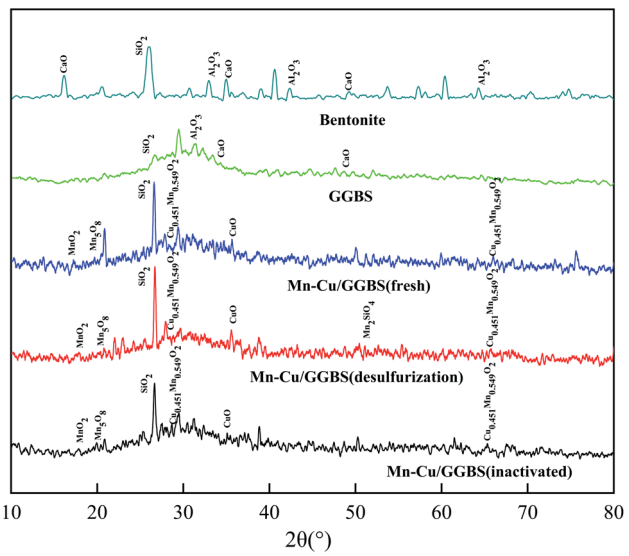

Fig. 2 XRD spectrum of the Mn–Cu/GGBS catalyst.

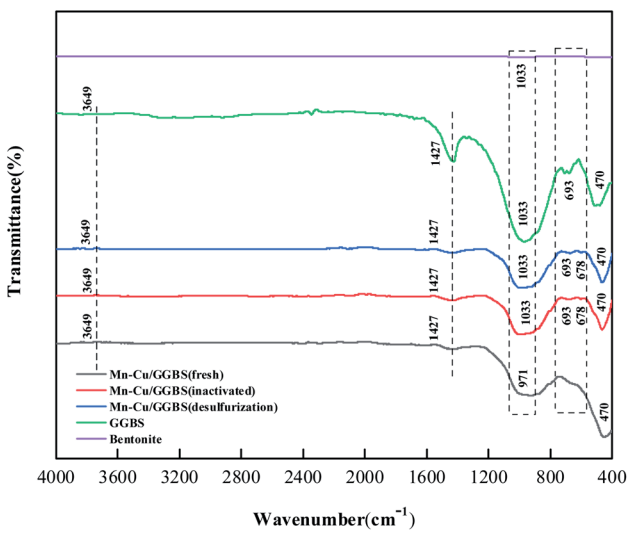

Fig. 3 FT-IR spectrum of the Mn–Cu/GGBS catalyst.

the high wavenumber. The Si–O–Si symmetric stretching vibration peak of $[Si_2O_7]^{6-}$ is located at 693 cm^{-1}. However, the shift of the peak towards a low wavenumber indicated that the degree of polymerization of the catalyst decreased and it became active. Because a large amount of CaO was contained in the slag, the vibration absorption peak of the gypsum phase appeared at 678 cm^{-1}. At 470 cm^{-1}, the bending vibration peak of Si–O–Si appeared in the slag. The catalyst peak moved

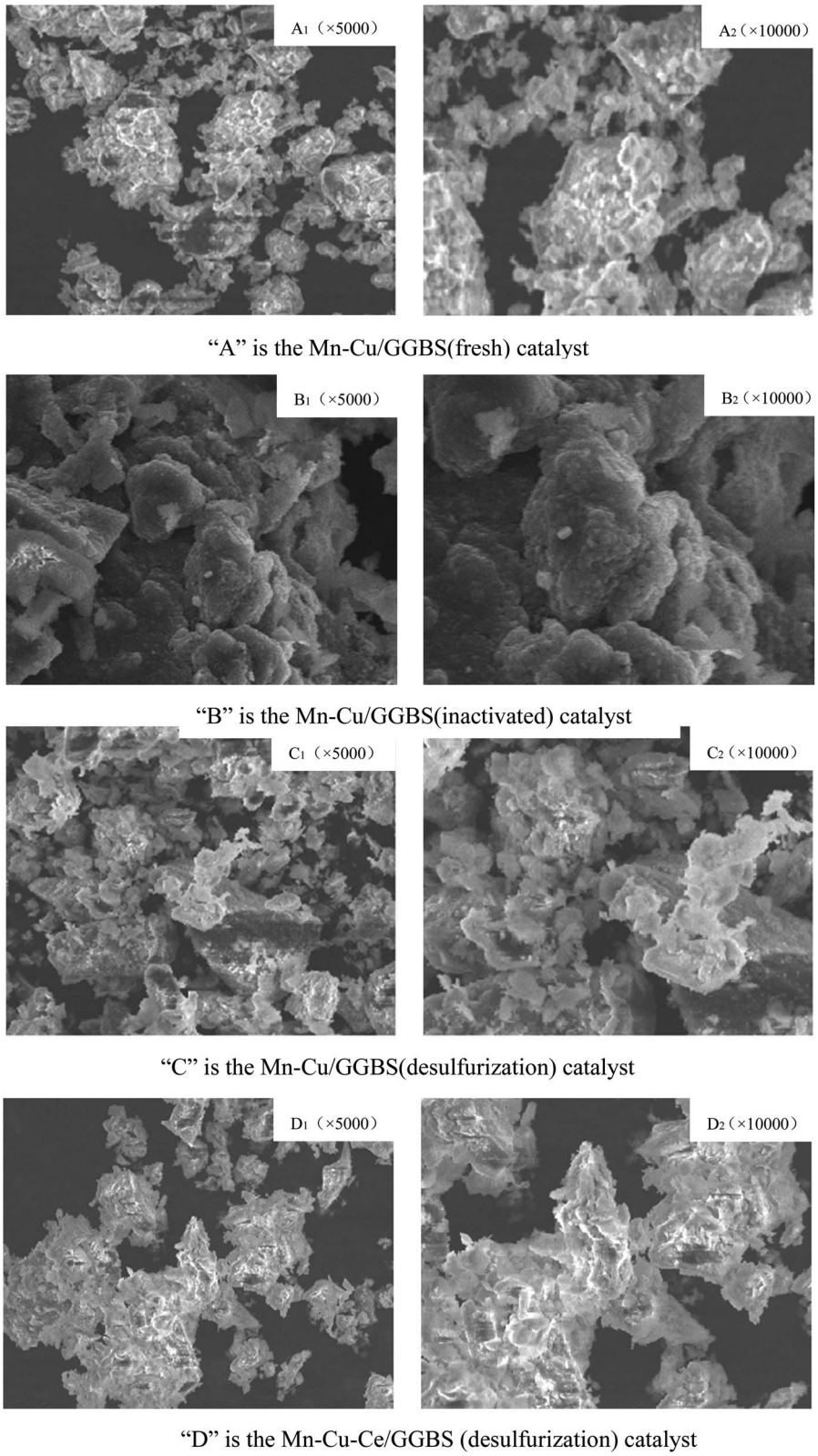

Fig. 4 (A)–(D) is the SEM images of Mn–Cu/GGBS and Mn–Cu–Ce/GGBS catalysts.

towards a lower wavenumber, and then the absorption peak became gradually sharper. It was the effect of cavitation during the modification of the ultrasonic-assisted metal salt. Consequently, there was friction between slag particles, which gradually became smaller and more active.

3.1.3 SEM analysis. As shown in Fig. 4, the electron microscope reflected different magnifications (10 000 and 5000 times) of the Mn–Cu/GGBS catalyst before and after denitration as well as after sulfur resistance. (A) is the Mn–Cu/GGBS (fresh) catalyst. (B) is the Mn–Cu/GGBS (inactivated) catalyst. (C) is the Mn–Cu/GGBS (desulfurization) catalyst. (D) is the Mn–Cu–Ce/GGBS (desulfurization) catalyst.

It can be seen from Fig. 4 that (A) is the Mn–Cu/GGBS (fresh) catalyst, and it passed through the high-temperature calcination stage, and the catalyst has just been formed. Therefore, the structure at the microscopic level is relatively loose. (B) is the Mn–Cu/GGBS catalyst (deactivated) after high temperature roasting. The active metal component impregnated on (A) is turned into metal oxide after high temperature roasting, which provides the basis for denitration and sulfur resistance. Under the catalysis of the active metal Mn–Cu, NO_x reduces nitrogen oxides to N_2 under the action of the reducing gas NH_3. (C) is the Mn–Cu/GGBS catalyst after desulfurization (desulfurization). During the reaction, ammonium sulfate is generated and concentrated on the surface of the catalyst, reducing the voids and pore structure between the catalyst particles. Therefore, the denitration activity of the catalyst is reduced, and it is finally got deactivated. In addition, (D) is the Mn–Cu–Ce/GGBS (desulfurization) catalyst, which, like the fresh catalyst, also produces an agglomerated structure. The reduction in voids between the agglomerated structures is due to the accumulation of sulfides and sulfates. There was a reaction between Mn and S elements, so that manganese sulfide as well as manganese sulfate were produced to reduce the activity of Mn element. At this moment, the reactive component Ce in the catalyst had a more active electronic layer structure than Mn, which first reacted with SO_2 to form cerium sulfide or cerium sulfate to protect the denitration performance of Mn. Therefore, the sulfur resistance of the Mn–Cu–Ce/GGBS catalyst was better than that of the Mn–Cu/GGBS catalyst after the introduction of the third reactive component Ce.

3.2. Catalytic properties of catalytic materials

The blast furnace slag was chosen as the main material, and the bimetallic supported blast furnace slag catalyst was prepared by equal volume impregnation. Mn was chosen as the first load metal and transition metals (Cr, Co, Ni, Cu, Zn, Ag, Cd, and Fe) as the second reactive component. The optimal bimetallic-supported blast furnace slag catalyst Mn–X/GGBS (X = Cr, Co, Ni, Cu, Zn, Ag, Cd, and Fe) was obtained by the denitration performance and characterization tests.

3.2.1 Tests for denitration and activity of the bimetallic-supported blast furnace slag-based catalyst. 8 groups of the blast furnace slag carrier were quantified, each of which was 10 g. Mn was chosen as the first load metal with 5% load and eight transition metals, namely Cr, Co, Ni, Cu, Zn, Ag, Cd, and Fe, were chosen as the second reactive component with 3% load, respectively. By the equal volume impregnation method, the carrier was impregnated in the configured solution for 24 h and then it was taken out, adjusting the temperature of the drying box at 105 °C, and the carrier after loading was placed in a constant temperature drying box for drying. There was about 15 min before it could be taken out. After setting the temperature of the muffle furnace as constant temperature, it was roasted in a muffle furnace with 450 °C for 2 h. Finally, the Mn–X/GGBS (X = Cr, Co, Ni, Cu, Zn, Ag, Cd, Fe) catalysts were prepared. The catalysts were used for the denitration experiment. The results are shown in Fig. 5.

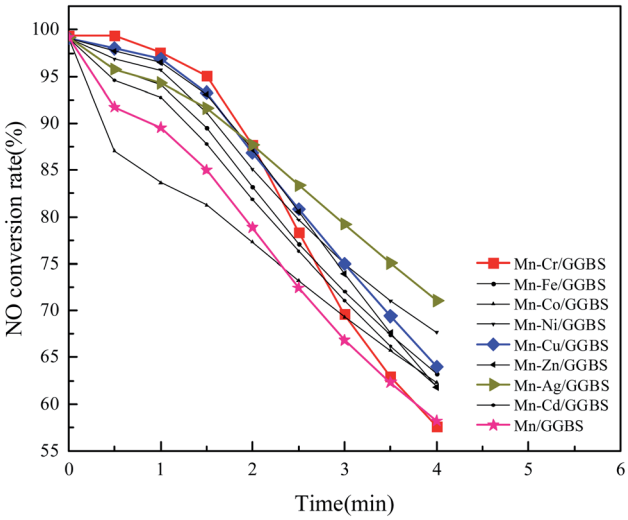

Fig. 5 The effect of the bimetallic (Mn–transition metal) load on the denitration performance of the blast furnace slag.

The results indicated the denitration effect at 150 °C and the first 2 min: Cr > Cu > Zn > Ni > Ag > Fe > Cd > Co. Compared to the Mn–Cu catalyst, the Mn–Ag bimetal supported blast furnace slag catalyst has better catalytic performance. However, the catalytic performance of the Mn–Ag bimetal supported blast furnace slag catalyst did not improve much. Also, Ag is expensive. According to a total comparison, the denitration rate of the blast furnace slag with the Mn–Cu bimetallic load was relatively slow, and its denitration effect was superior to that of other bimetallic supported catalysts. The denitration rate was still above 60% after 4 min. Moreover, it can be seen from Fig. 5 that the denitration performance of the bimetallic supported catalyst was obviously higher than that of the single component manganese-supported catalyst before deactivation. It means that the bimetallic-supported blast furnace slag could promote the denitration of the catalyst. The formed metal oxide was beneficial for denitration. The bimetallic co-impregnation was used to modify the blast furnace slag, so there were crystalline metal oxides except for MnO_x as well as CuO_x formed on the blast furnace slag after roasting by muffle furnace. Instead of adopting MnO_x alone, Mn–Cu/GGBS supported the catalyst to obtain better redox reactions and more surface acidic sites with the help of Cu and Mn. Besides, bimetallic oxide ($Cu_aMn_bO_x$) with a certain crystal structure would also increase the performance of the catalyst to some extent, which accelerated the NH_3–SCR reaction.

3.2.2 Tests for the sulfur resistance and the activity of the bimetallic supported blast furnace slag-based catalyst. Based on denitration, SO_2 was introduced to screen the catalysts with good denitration performance, so that the sulfur resistance could be tested. In industrial flue gas, except for nitrogen oxides, the flue gas that passes through the desulfurization system still leaves a small amount of sulfur dioxide, which is seriously harmful to the activity of the SCR catalyst at low temperature. There are two reasons: first, SO_2 is easily oxidized to become SO_3, which further mixes with NH_3 to produce $(NH_4)_2SO_3$, $(NH_4)_2SO_4$, and other compounds that deposit on the catalyst surface at low temperatures and encroach on the surface active sites of the catalyst. Naturally, the catalyst is easily deactivated. Second, SO_2 leads to the sulfonation of the active or support material on the catalyst surface, thereby deactivating the catalyst, such as the catalysts applied in industries. Consequently, significant attention must be paid to the sulfur resistance of the catalyst in practical applications. This section mostly describes the differences in the sulfur resistance of metal-supported catalysts. In the experiment, the quantity SO_2 was 160 ppm and N_2 was 452 mL min^{-1}. The rest of the conditions remained unchanged.

According to the results of the catalyst denitration in Fig. 5, Mn–Cr/GGBS, Mn–Cu/GGBS, and Mn–Zn/GGBS catalysts were quantified to be 10 g. These catalysts were put into a vertical furnace, and then SO_2 was added to conduct the sulfur resistance test. At this moment, the flue gas flux was 500 mL min^{-1}, O_2 30 mL min^{-1}, NO 8 mL min^{-1}, SO_2 2 mL min^{-1}, NH_3 8 mL min^{-1}, and the rest was filled with N_2. The effect of the bimetallic-supported catalysts on sulfur resistance was further obtained. The activity test results are shown in Fig. 6. According to the comparison, the denitration efficiency of the Mn–Cu/GGBS catalyst was better than that of the other two metal loads after SO_2 was infused, which was consistent with the results of the experiment described in Section 3.2.1. Obviously, the as-prepared Mn–Cu/GGBS catalyst possesses good denitration performance and anti-sulfur effect.

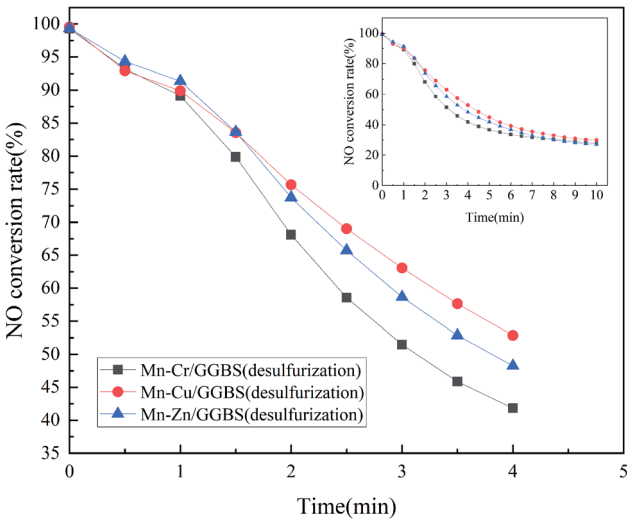

Fig. 6 Effect of bimetallic (Mn–transition metal) loading on sulfur resistance of the blast furnace slag.

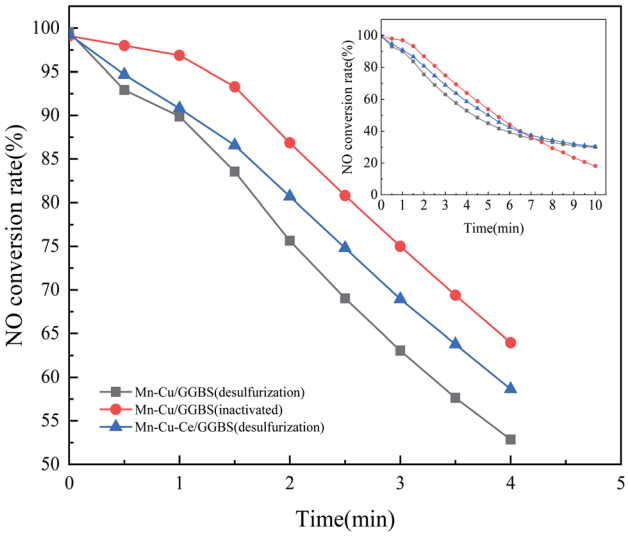

Fig. 7 Effect of tri-metallic (Mn–Cu–Ce) loading on the sulfur resistance of the blast furnace slag.

3.2.3 Test for sulphur resistance and activity of the trimetallic supported blast furnace slag-based catalyst. After comparing the results of the sulfur resistance of bimetallic loading, a third reactive component, Ce, was loaded simultaneously on the basis of optimal bimetallic loading, and thus the sulfur resistance of the blast furnace slag-based catalyst was further improved. According to the result of the sulfur resistance test of the catalysts in Fig. 6, the blast furnace slag carrier was quantified as 10 g. Mn was chosen as the first load metal with 5% load, the second was Cu with 3% load, and the third was Ce with 1% load. The carrier was impregnated in the configured solution for 24 h, adjusting the temperature of the drying box at 105 °C, and the carrier after loading was placed in a constant temperature drying box for drying. There was about 15 minutes before it could be taken out. After setting the temperature of the muffle furnace at constant temperature, it was roasted in a muffle furnace at 450 °C for 2 h. Finally, the Mn–Cu–Ce/GGBS catalyst was prepared.

The prepared catalyst was put into a vertical furnace and then SO_2 was added to conduct a sulfur resistance test. At this moment, the flue gas flux was 500 mL min^{-1}, O_2 was 30 mL min^{-1}, NO was 8 mL min^{-1}, SO_2 was 2 mL min^{-1}, NH_3 was 8 mL min^{-1}, and the rest was filled with N_2. The effect of the trimetallic supported catalyst on sulfur resistance was further obtained. The denitration results are shown in Fig. 7. After adding the third reactive component, Ce, the sulfur resistance of the Mn–Cu–Ce/GGBS catalyst was better than that of the Mn–Cu/GGBS catalyst. Obviously, the reactive component Ce accelerated the sulfur resistance against SO_2 of the catalyst.

4. Conclusion

In this study, the blast furnace slag from industrial waste was chosen as the main material, and a certain amount of calcium bentonite was added as the binder to prepare the catalyst

carrier. The authors worked out the denitration performance of a series of bimetallic and tri-metallic supported blast furnace slag catalysts by equal volume impregnation. In addition, a certain amount of SO_2 was introduced into the simulated flue gas system to investigate the sulfur resistance against SO_2 of the as-prepared catalyst. It was also analyzed by FT-IR, XRD, and SEM characterizations so as to not only determine the morphology, structures, and properties of the catalysts, but also analyze its denitration mechanism. The result indicated that it is feasible to use the blast furnace slag as the carrier of the denitration sulfur-resistant catalyst, which not only solves the problem of industrial waste pollution, but also achieves the aim of treating waste with waste and the recycling of waste. As an optimal bimetallic catalyst, Mn–Cu/GGBS possesses good denitration performance, and the NO conversion rate can reach up to 97%. Besides, it has sulfur resistance against SO_2. The sulfur resistance of the Mn–Cu–Ce/GGBS tri-metallic supported blast furnace slag catalyst is better than that of the bimetallic-supported blast furnace slag catalyst.

Conflicts of interest

None.

Acknowledgements

Shannxi Key Research and Development Project (2019ZDLSF05-05-01); 2019 Shaanxi Provincial Natural Science Basic Research Program Enterprise Joint Fund Project (2019JL-01); Xi'an Science and Technology Plan Project (2019217714GXRC013CG014-GXYD13.4); Open Fund of Shaanxi Key Laboratory of Geological Support for Coal Green Exploitation (DZBZ2020-08).

Notes and references

1 H. Wang, J. Wang, G. Z. Bo, S. G. Wu and L. T. Luo, *J. Cleaner Prod.*, 2020, **273**, 123019.
2 J. Wang, Z. N. Yang, H. Wang, S. G. Wu, H. Lu and X. G. Wang, *Sci. Total Environ.*, 2021, **758**, 143670.
3 Y. L. Shan, J. P. Du, Y. B. Yu, W. P. Yu and H. He, *Appl. Catal., B*, 2020, **266**, 118655.
4 C. X. Huang, G. L. Li, L. M. Yang and E. Ganz, *ACS Appl. Mater. Interfaces*, 2021, **13**, 608–621.
5 D. H. Jo, G. T. Park, T. Y. Ryu and S. B. Hong, *Appl. Catal., B*, 2019, **243**, 212–219.
6 C. Peng, R. Yan, H. G. Peng, Y. Y. Mi and F. D. Liu, *J. Hazard. Mater.*, 2020, **385**, 121593.
7 B. Y. Song, Y. Zhou, H. M. Yang, J. H. Liao, L. M. Yang, X. B. Yang and E. Ganz, *J. Am. Chem. Soc.*, 2019, **141**, 3630–3640.
8 M. G. Villa, A. Aranzabal and M. P. González-Marcos, *J. Ind. Eng. Chem.*, 2020, **81**, 440–450.
9 L. Zhang, Y. Jia, H. Shu, L. Zhang, X. Wen, M. Luo, Y. S. Wang and D. Xu, *Fuel*, 2020, **268**, 117242.
10 L. M. Yang, V. Bacic, L. A. Popov, A. L. Boldyrev, T. Heine, T. Frauenheim and E. Ganz, *J. Am. Chem. Soc.*, 2015, **137**, 2757–2762.
11 H. Wang, L. Zhang, Y. Tian, Y. Jia, G. Z. Bo, L. T. Luo and L. Liu, *Chemosphere*, 2021, **264**, 128456.
12 W. Z. Si, H. Y. Liu, T. Yan, H. Wang and J. H. Li, *Appl. Catal., B*, 2020, **269**, 312–326.
13 J. Yang, X. L. Wang, Y. T. Qu, X. Wang, H. Huo, Q. K. Fan, J. Wang, L. M. Yang and Y. Wu, *Adv. Energy Mater.*, 2020, **10**, 2001709.
14 L. Zhang, Y. Jia, L. Zhang, H. B. He, C. Yang, M. Luo and L. T. Miao, *J. Cleaner Prod.*, 2019, **217**, 317–323.
15 H. Wang, B. X. Quan, G. Z. Bo, Y. Z. Zhang, L. Liu, J. S. Zhang, X. Y. Zhang and C. H. Zhang, *J. Cleaner Prod.*, 2020, **267**, 122258.
16 J. H. Liu, L. M. Yang and E. Ganz, *ACS Sustainable Chem. Eng.*, 2018, **6**, 15494–15502.
17 S. H. Li, B. C. Huang and C. L. Yu, *Catal. Commun.*, 2017, **98**, 47–51.
18 Y. C. Choi, J. Y. Kim and S. C. Choi, *Constr. Build. Mater.*, 2017, **137**, 96–103.
19 J. H. Liu, L. M. Yang and E. Ganz, *J. Mater. Chem. A*, 2019, **7**, 3805–3814.
20 L. Zhang, H. Shu, Y. Jia, L. Zhang and D. Xu, *Int. J. Hydrogen Energy*, 2020, **45**, 19280–19290.
21 A. Kubilay, A. Semiha and A. Abdullah, *Journal of Civil Engineering and Management*, 2018, **22**, 2994–3002.
22 J. H. Liu, L. M. Yang and E. Ganz, *J. Mater. Chem. A*, 2019, **7**, 11944–11952.
23 Y. H. Li, F. M. Chang, B. Huang, Y. P. Song, H. Y. Zhao and K. J. Wang, *Fuel*, 2020, **266**, 117063.
24 L. Zhang, H. Shu, L. Zhang and Y. Jia, *ACS Omega*, 2020, **5**, 14911–14923.
25 J. H. Liu, L. M. Yang and E. Ganz, *RSC Adv.*, 2019, **9**, 27710–27719.
26 P. Itthikorn, H. Suksun, R. Runglawan, A. Arul and P. Prinya, *J. Hazard. Mater.*, 2018, **341**, 257–267.
27 A. R. Hugo, C. R. Juan, F. P. Daniel, A. V. Hermes, A. R. Fredy, D. Farias and M. Muniz, *J. Mater. Civ. Eng.*, 2018, **30**, 04018244.
28 L. Xu, L. M. Yang and E. Ganz, *Theor. Chem. Acc.*, 2018, **137**, 98.
29 Q. Song, H. Y. Zhao, J. W. Jia, Q. Y. Li, W. Lv, Q. X. Gu and X. Q. Shu, *J. Anal. Appl. Pyrolysis*, 2020, **145**, 104716.
30 L. Zhang, H. Gao, X. Chang, Z. Lei, X. Wen and Y. S. Wang, *J. Cleaner Prod.*, 2020, **249**, 119307.
31 J. J. Wu, H. Wang, X. Zhu, Q. Liao and K. Li, *Appl. Therm. Eng.*, 2017, **111**, 1557–1564.
32 M. Spanka, T. Mansfeldt and R. Bialucha, *Environ. Sci. Pollut. Res.*, 2018, **25**, 23082–23090.
33 L. Zhang, J. H. Chen, L. Zhang, H. B. He, Y. S. Wang and Y. H. Li, *J. Cleaner Prod.*, 2019, **225**, 220–226.
34 M. Z. Wu, H. H. Lua, M. C. Liu, Z. L. Zhang, X. R. Wu, W. M. Liu, P. Wang and L. S. Li, *Hydrometallurgy*, 2017, **167**, 8–15.
35 R. Tong, Z. Sun, X. N. Wang, L. M. Yang, J. W. Zhai, S. P. Wang and H. Pang, *Int. J. Hydrogen Energy*, 2020, **45**, 18912–18921.
36 Q. Song, H. Y. Zhao, J. W. Jia, Q. Y. Li, L. Wen, J. W. Bao, X. Q. Shu, Q. X. Gu and P. Zhang, *J. Cleaner Prod.*, 2020, **258**, 120628.

37 L. Zhang, L. B. Qi, H. Shu, Y. Jia, L. Zhang, C. Yang, F. Bai and Z. F. Sun, *ACS Omega*, 2020, **5**, 31567–31574.
38 D. M. Meng, Q. Xu, Y. L. Jiao, Y. Gao, Y. L. Wang, L. Li, G. Z. Zhan and C. Wang, *Appl. Catal., B*, 2018, **221**, 652–663.
39 J. H. Liu, L. M. Yang and E. Ganz, *Energy Environ. Mater.*, 2019, **2**, 193–200.
40 L. Zhang, H. Shu, Y. Jia, Z. Lei, F. Bai, W. Kuang, L. B. Qi, J. Shang and C. Wei, *Chemosphere*, 2020, 128646.
41 Q. Song, H. Zhao, S. Q. Chang, L. Yang, F. Zou, X. Q. Shu, Q. Gu and P. Zhang, *J. Anal. Appl. Pyrolysis*, 2020, **151**, 104927.
42 H. Y. Zhao, Y. H. Li, Q. Song, S. C. Liu, Q. X. Ma, M. Li and X. Q. Shu, *Fuel*, 2020, **286**, 119398.
43 J. C. Chen, J. H. Zhang, J. Y. Liu and H. Yao, *Chem. Eng. J.*, 2020, **397**, 125372.
44 H. Y. Zhao, Q. Song, S. C. Liu, Y. H. Li, X. H. Wang and X. Q. Shu, *Energy Environ. Mater.*, 2018, **161**, 13–26.
45 J. H. Zhang, G. Sun, J. Y. Liu, F. Evrendilek and M. Buyukada, *J. Cleaner Prod.*, 2020, **253**, 119950.